CLM-P783

CLM-P783

UKAEA

Preprint

FOKKER-PLANCK STUDIES OF HIGH POWER ELECTRON CYCLOTRON HEATING IN TOKAMAKS

M. R. O'BRIEN
M. COX
D. F. H. START

CULHAM LABORATORY
Abingdon, Oxfordshire
1986

CLM-P 783

FOKKER-PLANCK STUDIES OF HIGH POWER ELECTRON CYCLOTRON HEATING IN TOKAMAKS

M R O'Brien, M Cox and D F H Start

Culham Laboratory, Abingdon, Oxon, OX14 3DB, UK
(Euratom/UKAEA Fusion Association)

ABSTRACT

A Fokker-Planck formalism has been developed to interpret experimental data from high power electron cyclotron heating of tokamak plasmas in which the electron distribution function can be substantially distorted. The Fokker-Planck equation is solved using a 2-D code which incorporates electron trapping, a steady ohmic electric field and a bounce-averaged electron cyclotron heating term. The quasi-linear RF diffusion coefficient is calculated using a single particle model which includes the mildly relativistic resonance condition and takes into account localised RF power injection and tokamak rotational transform effects. Comparisons are presented of the calculated and observed soft X-ray spectra from 60 GHz second harmonic electron cyclotron heating experiments on the CLEO tokamak. Good agreement between theory and experiment is found. In addition, predicted RF current drive efficiencies for the COMPASS tokamak are presented.

(Submitted for publication in Nuclear Fusion)

June 1986
cmk

FOKKER-PLANCK STUDIES OF HIGH POWER ELECTRON CYCLOTRON HEATING IN TOKAMAKS

M R O'Brien, M Cox and D F H Start

Culham Laboratory, Abingdon, Oxon OX14 3DB, UK
(Euratom/UKAEA Fusion Association)

ABSTRACT

A Fokker-Planck formalism has been developed to interpret experimental data from high power electron cyclotron heating of tokamak plasmas in which the electron distribution function can be substantially distorted. The Fokker-Planck equation is solved using a 2-D code which incorporates electron trapping, a steady ohmic electric field and a bounce-averaged electron cyclotron heating term. The quasi-linear RF diffusion coefficient is calculated using a single particle model which includes the mildly relativistic resonance condition and takes into account localised RF power injection and tokamak rotational transform effects. Comparisons are presented of the calculated and observed soft X-ray spectra from 60 GHz second harmonic electron cyclotron heating experiments on the CLEO tokamak. Good agreement between theory and experiment is found. In addition, predicted RF current drive efficiencies for the COMPASS tokamak are presented.

1 INTRODUCTION

The use of electron cyclotron waves as a source of additional heating for tokamak research has now reached the Megawatt power level in the T10 and Doublet III tokamaks[1-2] and experiments at even higher powers are anticipated in the near future[3]. Such intense heating is expected to produce significantly non-thermal electron distributions (eg enhanced trapped electron populations) which might be beneficial for confinement, as in lower hybrid heating experiments[4], and could improve β-limits and MHD stability[5]. Distorted distributions will also modify the interpretation of data from X-ray, Thomson scattering and electron cyclotron emission diagnostics. Some of these effects have already been observed. For example, anisotropic electron distributions and improved confinement times have been produced in low density plasmas

on the TOSCA and CLEO tokamaks by injecting 28 GHz, second harmonic X-mode radiation from the low field side[6-7]. Similar distorted distributions have also been observed on the PDX tokamak[8]. In addition, evidence for enhanced particle trapping has been seen on the TOSCA[9-10], T10[11] and PDX[8] machines.

In order to understand these phenomena which depend on details of the electron distribution function we have developed a Fokker-Planck code which can treat the strong distortions produced when the RF-induced diffusion exceeds the collisional diffusion by up to an order of magnitude. The code is two dimensional in velocity space, calculates the distribution function on a given flux surface and incorporates a) trapped particles by solving the bounce-averaged Fokker-Planck equation and b) the steady toroidal electric field used for ohmic heating. The electron cyclotron resonance heating (ECRH) is modelled by a quasi-linear diffusion operator which is averaged over a flux surface and includes the effects of finite RF beam width, tokamak rotational transform, and a resonance condition which allows for the relativistic dependence of the cyclotron frequency on electron speed. The limitations of the quasi-linear approach are discussed in sections 3.1 and 5.2. Principally in respect of its treatment of trapped particles and bounce-averaging of the quasi-linear diffusion coefficient, the code is an improvement over previous tokamak calculations [12-17]. Similar considerations have been applied to ECRH in mirrors[18-19] and the Livermore bounce-averaged ICRF code is presently being adapted to ECRH[20].

The paper is arranged as follows. In Section 2 the bounce-averaged Fokker-Planck equation is defined along with the collision and electric field terms. The form of the ECRH quasi-linear diffusion operator in toroidal geometry is obtained in the first part of Section 3 by considering changes in the constants of motion of the unperturbed electron orbits. Then the diffusion coefficient due to the RF is calculated using a single particle model and is suitably averaged over the electron bounce phase. The last part of Section 3 deals with the possibility of the electrons being heated out of resonance before they can completely cross the RF beam. This effect plays an important role for resonant electrons with low parallel velocities, such as trapped electrons which come into resonance close to the turning points of their 'banana' orbits. In Section 4 we discuss the boundary conditions and the method used to solve the Fokker-Planck equation. In Section 5 some results are presented in the form of electron distribution functions and current drive efficiencies. Predicted soft X-ray spectra are also compared with data from ECRH experiments on the CLEO tokamak.

2 THE BOUNCE-AVERAGED FOKKER-PLANCK EQUATION

Symbolically we write the Fokker-Planck equation for electrons on a given flux surface averaged over the particle bounce time as

$$\frac{\partial f}{\partial t} = \langle(\frac{\partial f}{\partial t})_C\rangle + \langle(\frac{\partial f}{\partial t})_W\rangle + \langle(\frac{\partial f}{\partial t})_E\rangle \qquad (1)$$

where the terms on the r.h.s. are due to collisions, RF wave induced diffusion and the steady toroidal electric field respectively. The angular brackets denote the average over particle orbit

$$\langle A\rangle = (\oint \frac{d\chi}{v_\parallel})^{-1} \oint A \frac{d\chi}{v_\parallel} \qquad (2)$$

where χ is the poloidal angle and $v_\parallel$ is the electron velocity parallel to the magnetic field lines.

The collision term is expressed in flux conserving form using the expression

$$(\frac{\partial f}{\partial t})_C = \frac{e^4 n_e \ell n\lambda}{4\pi\varepsilon_0^2 m^2} \nabla\cdot\{-f\nabla h + \tfrac{1}{2}\nabla\cdot(f\nabla\nabla g)\} \qquad (3)$$

where h and g are the Rosenbluth potentials[21] for electron-electron and electron-ion scattering, n_e is the electron density, $\ell n\lambda$ is the Coulomb logarithm and m is the electron mass. In the present calculations we linearize the electron-electron collision term by taking a drifting Maxwellian for the field particle distribution in the calculation of h and g. As shown by Fisch and Karney[22] the drift ameliorates the approximation of not using the full non-linear collision operator with the potentials derived from f. With this assumption the collision term becomes

$$\langle(\frac{\partial f}{\partial t})_C\rangle = \nu_0 \{\frac{1}{x^2}\frac{\partial}{\partial x}(P+Q) + \frac{1}{r}\frac{1}{x\sin\theta_0}\frac{\partial}{\partial\theta_0}(R+S)\} \qquad (4)$$

where x is the electron speed v divided by the thermal speed v_e, θ_0 is the pitch angle of the electron as it passes through the midplane on the outside of the tokamak (χ=0) and

$$P = \frac{\Lambda}{2x}\frac{\partial f}{\partial x} + \Lambda f \qquad (5)$$

$$Q = v_d r^{-1} u \left|\cos\theta_0\right| \{ \left(\frac{3\Lambda}{2x^2} - x\phi'\right)\frac{\partial f}{\partial x} + 2\left(\frac{\Lambda}{x} - x^2\phi'\right) f - \frac{1}{2x}\tan\theta_0\left(\phi - \frac{3\Lambda}{2x^2}\right)\frac{\partial f}{\partial \theta_0}\} \quad (6)$$

$$R = \frac{t}{2}\sin\theta_0\left(\frac{\phi}{x^2} - \frac{\Lambda}{2x^4} + \frac{Z}{x^2}\right)\frac{\partial f}{\partial \theta_0} \quad (7)$$

$$S = v_d x^{-3}\left|\cos\theta_0\right|\sin\theta_0\{\frac{s}{2}\left(\phi - \frac{3\Lambda}{2x^2}\right)\frac{\partial f}{\partial \theta_0} + u\Lambda\tan\theta_0 f - \frac{u}{2}\tan\theta_0\left(x\phi - \frac{3\Lambda}{2x}\right)\frac{\partial f}{\partial x}\} \quad (8)$$

$$r = \left|\cos\theta_0\right| \oint \frac{d\chi}{\cos\theta} \quad (9)$$

$$s = \oint \frac{B(o)}{B(\chi)}\frac{\cos^2\theta}{\cos^2\theta_0} d\chi \quad (10)$$

$$t = \oint \frac{B(0)}{B(\chi)}\cos\theta\, d\chi / \left|\cos\theta_0\right| \quad (11)$$

$$u = \oint d\chi \quad (12)$$

$$\phi(x) = \frac{2}{\pi^{\frac{1}{2}}}\int_0^x e^{-y^2} dy \quad (13)$$

$$\Lambda = \phi - x\phi' \quad (14)$$

$$\nu_0 = e^4 n_e \ell n\lambda / 4\pi\varepsilon_0^2 v_e^3 m^2 \quad (15)$$

In the above equations v_d is the drift speed of the field particles normalised to v_e, Z is the effective charge of the plasma ions, $B(\chi)$ and $B(o)$ are the values of the magnetic field at poloidal angle χ and on the outer midplane ($\chi=0$) respectively, θ is the local electron pitch angle at poloidal angle χ and the thermal velocity v_e is related to the temperature T_e by $v_e = (2T_e/m)^{\frac{1}{2}}$. The integrals around the particle orbits depend on the class of particle considered and are defined as

$$\oint A(\sigma,\chi)dx = \left\{ \begin{array}{l} \frac{1}{\pi}\int_0^{\pi} A(\sigma,\chi)d\chi \text{ for co-passing electrons, } v_{\parallel}>0 \\ \frac{1}{\pi}\int_{\pi}^{0} A(\sigma,\chi)d\chi \text{ for counter-passing electrons, } v_{\parallel}<0 \\ \frac{1}{\pi}\sum_{\sigma}\int_0^{\chi_t} \sigma A(\sigma,\chi)d\chi \text{ for trapped electrons,} \end{array} \right\} \quad (16)$$

for axisymmetric systems and equilibria in which $|B|$ varies monotonically around the flux surfaces between $\chi=0$ and $\chi=\pi$.

The angle χ_t is the poloidal angle at the upper tip of the 'banana' orbit ($0<\chi_t<\pi$) and $\sigma = v_\parallel/|v_\parallel|$. Note that $u=\oint d\chi = +1$ for co-passing electrons, $u= -1$ for counter-passing electrons, and that $u=s=Q=S=0$ for trapped electrons. The drift speed v_d is determined by the condition that no force exists between f and the drifting Maxwellian.

The electric field term in eq (1) is given by

$$\left\langle \left(\frac{\partial f}{\partial t}\right)_E \right\rangle = -\left\langle \frac{eE}{m}\frac{\partial f}{\partial v_\parallel} \right\rangle$$

$$= -\frac{eE}{mv_e}\frac{u}{r}\left|\cos\theta_0\right|\left\{\frac{1}{x^2}\frac{\partial}{\partial x}(x^2 f) - \frac{\sec\theta_0}{x\sin\theta_0}\frac{\partial}{\partial\theta_0}(\sin^2\theta_0 f)\right\} \quad (17)$$

3. The RF Diffusion Term

In Section 3.1 we determine the form of the quasi-linear diffusion operator $\left\langle\left(\frac{\partial f}{\partial t}\right)_w\right\rangle$ for tokamak geometry starting from the general expression given by Laval and Pellat[23] in terms of the constants of the unperturbed motion. Then, in Section 3.2 we obtain the elements of the diffusion tensor using a single particle model similar to those used by Fielding[24] and by Cairns and Lashmore-Davies[25]. This approach enables us to take into account, in a physically transparent manner, the finite size of the microwave input beam, the variation of both the cyclotron frequency and the parallel velocity of the particle as it moves along the field lines, the attenuation of the wave as it propagates and the heating out of resonance of electrons before they can completely cross the RF beam. This last effect is due to the relativistic mass increase as the electrons gain energy and is particularly important for electrons with a small parallel velocity component.

3.1 The Quasi-linear Diffusion Operator in Toroidal Geometry

For a uniform magnetic field $\left(\frac{\partial f}{\partial t}\right)_w$ is given by

$$\left(\frac{\partial f}{\partial t}\right)_w = \frac{1}{v_\perp}\frac{\partial}{\partial v_\perp}\left\{v_\perp D_o \frac{\partial f}{\partial v_\perp}\right\} \quad (18)$$

in which $v_\perp$ is the component of the electron velocity perpendicular to the magnetic field and D_o is the quasi-linear diffusion coefficient. In the single particle model D_o is found by calculating the increment in perpendicular velocity, $\Delta v_\perp$, as an electron passes through the beam. The diffusion coefficient is then obtained from the expression

$$D_o = \frac{1}{2} [(\Delta v_\perp)^2]/\Delta t \tag{19}$$

where the square brackets denote the average over initial gyrophase angle and Δt is the mean time between successive transits through the beam. Equation (19) is valid provided $\Delta v_\perp$ is less than the gradient scale length of the distribution function in perpendicular velocity[26]. Using eq (5.42) of ref 26 and taking the distribution to be Maxwellian we obtain the criterion

$$\left(\frac{2\,\Delta v_\perp\, v_\perp}{v_e^2}\right)^2 << 1 \tag{20}$$

To some extent eq (20) is too restrictive on $\Delta v_\perp$ since the gradient of the distribution function in the resonance region will be less than that for a Maxwellian due to the diffusion in $v_\perp$.

In the case of an inhomogeneous magnetic field the wave particle interaction is described by the more general expression given by Laval and Pellat[23] namely

$$\left\langle \left(\frac{\partial f}{\partial t}\right)_w \right\rangle = \frac{1}{2} \frac{\partial}{\partial J_i} \left\{ \left\langle \left[\frac{\Delta J_i \Delta J_j}{\Delta t}\right] \right\rangle \frac{\partial f}{\partial J_j} \right\} \tag{21}$$

with summations over repeated indices. The quantities J_i are constants of the unperturbed motion and the products $\Delta J_i\ \Delta J_j$ are averaged over the cyclic variables which are canonically conjugate to the actions J_i. We use the set of action-angle variables given by Taylor[27] and by Kaufman[28], namely $(\mu, \theta_g; J, \Phi; a, b)$ where $\mu = v_\perp^2/2B$, θ_g is the gyrophase, $J = \oint v_\parallel d\chi$, Φ is the bounce phase defined by $\Phi = \int_0^\chi v_\parallel^{-1} d\chi / \oint v_\parallel^{-1} d\chi$, and a and b label each field line. In this work we keep a and b constant so that we do not take into account the finite radial widths of the banana orbits or differentiate between drift and flux surfaces for the passing particles. This is usually a good approximation for electrons. For example 10 keV electrons typically drift ~3mm from the flux surfaces in the CLEO tokamak. Thus eq (21) becomes

$$\left\langle \left(\frac{\partial f}{\partial t}\right)_w \right\rangle = \frac{\partial}{\partial \mu} \left\{ \frac{\left\langle [(\Delta\mu)^2] \right\rangle}{2\Delta t} \frac{\partial f}{\partial \mu} + \frac{\left\langle [\Delta\mu \Delta J] \right\rangle}{2\Delta t} \frac{\partial f}{\partial J} \right\}$$
$$+ \frac{\partial}{\partial J} \left\{ \frac{\left\langle [\Delta\mu \Delta J] \right\rangle}{2\Delta t} \frac{\partial f}{\partial \mu} + \frac{\left\langle [(\Delta J)^2] \right\rangle}{2\Delta t} \frac{\partial f}{\partial J} \right\} \tag{22}$$

where the square brackets denote the gyrophase averages and the angular

brackets the bounce phase average. This equation is in divergence form and the terms in curly brackets can be thought of as contravariant components of a flux $\underline{S}$, ie

$$\left(\frac{\partial f}{\partial t}\right)_w = \frac{\partial S^\mu}{\partial \mu} + \frac{\partial S^J}{\partial J} \tag{23}$$

Transforming eq (22) from (μ,J) variables to (v,θ_0) variables we have

$$\left\langle\left(\frac{\partial f}{\partial t}\right)_w\right\rangle = \frac{1}{v^2}\frac{\partial}{\partial v}\{v^2 S^v\} + \frac{1}{\langle v_{\parallel_0}/v_\parallel\rangle \sin\theta_0}\frac{\partial}{\partial \theta_0}\{\sin\theta_0 \langle v_{\parallel_0}/v_\parallel\rangle S^{\theta_0}\} \tag{24}$$

where the new components of $\underline{S}$ are given by

$$\begin{pmatrix} S^v \\ S^{\theta_0} \end{pmatrix} = \underline{V} \cdot \begin{pmatrix} S^\mu \\ S^J \end{pmatrix} \tag{25}$$

where $\underline{V} = \begin{pmatrix} v_\mu & v_J \\ \theta_{0\mu} & \theta_{0J} \end{pmatrix}$ and $v_\mu = \frac{\partial v}{\partial \mu}$ etc. in standard notation. From the expressions

$$J = v\oint_\sigma \left\{1 - \frac{B(\chi)}{B(o)}\sin^2\theta_0\right\}^{-\frac{1}{2}} d\chi \tag{26}$$

and

$$\mu = \frac{v^2}{2B(o)}\sin^2\theta_0 \tag{27}$$

we obtain

$$v_\mu = \langle B(\chi)\rangle / v \tag{28}$$

$$v_J = v_{\parallel_0}/(rv) \tag{29}$$

$$\theta_{0\mu} = v^{-2}\tan\theta_0 \left\langle\left\{\frac{B(o)}{\sin^2\theta_0} - B(\chi)\right\}\right\rangle \tag{30}$$

$$\theta_{0J} = \sin\theta_0/(rv) \tag{31}$$

for both the passing and trapped electrons. In deriving the equations for the trapped particles we have used the fact that the integrands appearing in the bounce averages are zero at the velocity-space dependent limits of the integral.

We now require the components S^v and S^{θ_0} in eq (25) in terms of $\frac{\partial f}{\partial v}$ and $\frac{\partial f}{\partial \theta_0}$. Using eqs(22, 23 and 25) and expressing $\frac{\partial f}{\partial \mu}$ and $\frac{\partial f}{\partial J}$ in terms of $\frac{\partial f}{\partial v}$ and $\frac{\partial f}{\partial \theta_0}$ we obtain

$$\begin{pmatrix} S^{v} \\ S^{\theta_0} \end{pmatrix} = \underline{V}\,\underline{D}\,\underline{V}^{T} \begin{pmatrix} \frac{\partial f}{\partial v} \\ \frac{\partial f}{\partial \theta_0} \end{pmatrix} \tag{32}$$

where $\underline{D} = \begin{pmatrix} D_{\mu\mu} & D_{J\mu} \\ D_{\mu J} & D_{JJ} \end{pmatrix}$ (33)

and $D_{\mu J} = <[\Delta\mu\Delta J]>/(2\Delta t)$ etc. (34)

Equations (24) and (32) thus give $<(\frac{\partial f}{\partial t})_{w}>$ in a form which is appropriate for inclusion in the Fokker-Planck equation (eq(1)) in which the collision and electric field terms are given by eq (4) and eq (17) respectively. The coefficients $D_{\alpha\beta}$ can be calculated from the increment in $v_{\perp}$ produced by the wave-particle interaction using the following relationships.

$$D_{\mu\mu} = v_{\perp_0}^{2} \{B_R B(o)\}^{-1} D_o \tag{35}$$

$$D_{\mu J} = D_{J\mu} = v_{\perp_0}^{2} B(o)^{-1} \{\oint (1 - \frac{B(\chi)}{B_R}) v_{\parallel}^{-1} d\chi\} D_o \tag{36}$$

$$D_{JJ} = v_{\perp_0}^{2} B_R B(o)^{-1} \{\oint (1 - \frac{B(\chi)}{B_R}) v_{\parallel}^{-1} d\chi\}^{2} D_o \tag{37}$$

where $D_o = <[(\Delta v_{\perp})^2]>/2\Delta t$ and B_R is the magnetic field at the point where the electron crosses the radio frequency beam.

3.2 The Calculation of the Diffusion Coefficient D_o

The calculation of $<[(\Delta v_{\perp})^2]>$ is based on the earlier work of Fielding[24] and of Cairns and Lashmore-Davies[25] and proceeds by finding the gyrophase averaged square of the increment in perpendicular velocity for an electron making a single pass through the RF beam. The equation for the electron motion is

$$\frac{d\underline{v}}{dt} = -\frac{e}{m} \{\underline{\tilde{E}} + \underline{v} \times (\underline{B} + \underline{\tilde{B}})\} \tag{38}$$

where $\underline{\tilde{E}}$ and $\underline{\tilde{B}}$ are the oscillating electric and magnetic fields respectively and $\underline{B}$ is the steady magnetic field of the tokamak. The component equations of (38) for the motion perpendicular to $\underline{B}$ are the real parts of the equations

$$\frac{dV_x}{dt} = -\frac{e}{m}\tilde{E}_x - i\Omega V_y \tag{39}$$

$$\frac{dV_y}{dt} = -\frac{e}{m}\tilde{E}_y + i\Omega V_x \tag{40}$$

in which V_x, V_y, are complex variables and Ω is the gyrofrequency. We have neglected the $\underline{v} \times \underline{\tilde{B}}$ terms in eqs (39) and (40) for clarity. The full expression for $(\Delta v_\perp)^2$ including these terms is given towards the end of this section. The real velocities v_x and v_y are related to V_x and V_y as follows

$$v_x = v_\perp \cos\phi = \mathrm{Re}V_x \tag{41}$$

$$v_y = v_\perp \sin\phi = \mathrm{Re}V_y \tag{42}$$

in which ϕ is the gyrophase and is related to the initial gyrophase ϕ_0 by the equation

$$\phi(t) = \int_{-\infty}^{t} \Omega dt' + \phi_0 \tag{43}$$

We take the wave field to have the form

$$\tilde{\underline{E}} = \underline{E}(\underline{r}) \exp(-i\omega t + i\underline{k}.\underline{r}) \tag{44}$$

where $\underline{k}$ is the wavevector and $\underline{r}$ is the electron position vector. In general the components of $\underline{E}(\underline{r})$ are complex to describe the various possible states of polarization. Defining $V_\pm = V_x \pm iV_y$ and $E_\pm = E_x \pm iE_y$ we can write eqs(39) and (40) as

$$\frac{dV_\pm}{dt} \mp i\Omega V_\pm = -\frac{e}{m} E_\pm \exp(-i\omega t + i\underline{k}.\underline{r}) \tag{45}$$

which can be integrated to give

$$V_\pm(\infty)e^{\mp i\phi(\infty)} = V_\pm(-\infty)e^{\mp i\phi_0} + G_\pm \tag{46}$$

where

$$G_\pm = -\frac{e}{m}\int_{-\infty}^{\infty} E_\pm \exp\{-i\omega t + i\underline{k}.\underline{r} \mp i\phi\}\, dt \tag{47}$$

We now consider the wave to be pure right hand circularly polarised ($E_+ = 0$) and so

$$V_+(\infty) = e^{i(\phi(\infty)-\phi_0)}\, V_+(-\infty) = 0 \tag{48}$$

The perpendicular velocity squared is given in terms of V_- by

$$v_\perp^2 = \tfrac{1}{4}\, V_- V_-^* \tag{49}$$

Consequently the increment in $v_\perp^2$ is given by

$$\Delta(v_\perp^2) = \tfrac{1}{4}\,\{V_-(\infty)V_-^*(\infty) - V_-(-\infty)V_-^*(-\infty)\} \tag{50}$$

which leads to the following expression for $\Delta v_\perp$

$$\Delta v_\perp = \tfrac{1}{2}\, v_\perp^{-1}\, \Delta(v_\perp^2) = \{V_-(-\infty)G_-^* e^{i\psi_0} + V_-^*(-\infty)G_- e^{-i\psi_0}\}/8v_\perp \tag{51}$$

The evaluation of G_- proceeds by writing eq (47) as

$$G_- = -\frac{e}{m}\int_{-\infty}^{\infty} E_- \exp\{i(-\omega t + k_\parallel \int_{-\infty}^{t} v_\parallel dt' + \frac{k_\perp v_\perp}{\Omega}\sin\phi + i\phi)\}\, dt \tag{52}$$

Expanding the term $\exp\,(i\frac{k_\perp v_\perp}{\Omega}\sin\phi)$ in terms of Bessel functions we find

$$G_- = -\frac{e}{m}\sum_{\ell=-\infty}^{\infty} e^{i\ell\psi_0}\int_{-\infty}^{\infty} J_{\ell-1}(\frac{k_\perp v_\perp}{\Omega})\, E_- \exp\{i(-\omega t + k_\parallel \int_{-\infty}^{t} v_\parallel dt' + \ell\int_{-\infty}^{t}\Omega dt')\}\, dt \tag{53}$$

Substituting this expression for G_- into eq (51), noting that $V_-(-\infty) = 2v_\perp e^{-i\psi_0}$ and using the small argument expansion of the Bessel function ($k_\perp v_\perp/\Omega \lesssim 0.5$) we obtain the following expression for $(\Delta v_\perp)^2$ averaged over the initial gyrophase ψ_o

$$[(\Delta v_\perp)^2] = \frac{1}{8}\left(\frac{e}{m}\frac{1}{(\ell-1)!}\right)^2 \left|\int_{-\infty}^{\infty} (\frac{k_\perp v_\perp}{2\Omega})^{(\ell-1)} E_-(\underline{r})\, \exp\,\{i(-\omega t + k_\parallel\int_{-\infty}^{t} v_\parallel dt' + \ell\int_{-\infty}^{t}\Omega dt')\}\, dt\right|^2 \tag{54}$$

for heating at harmonic number ℓ. The contribution to $(\Delta v_\perp)^2$ due to an E_+ component is much less than that given by eq(54) since it contains an extra factor $(k_\perp v_\perp/\Omega)^4$. If we keep the $\underline{v} \times \underline{B}$ terms in eqs (39) and

(40) then the essential modification is that $E_-(\underline{r})$ in eq(54) is replaced by $E_- + (k_\perp v_\parallel/\omega)E_z$.

The next step is to evaluate the single pass $[(\Delta v_\perp)^2]$ given by eq (54) by specifying the spatial dependence of the wave field $E_-(\underline{r})$ and the time dependence of Ω and the particle velocity. This is done using the model shown in Fig 1 in which a beam of microwave power is injected into a tokamak in the mid-plane and at an angle α to the magnetic axis. The injected beam is taken to have a Gaussian profile which is symmetric about the beam axis and each ray is assumed to suffer the same absorption in propagating to a given value of the major radius R. Such a profile simulates reasonably well the radiation pattern of the TE_{11} mode from a circular antenna[29] which is being used on CLEO experiments. Thus in terms of the coordinate system shown in Fig.1 we can write

$$E_-(\underline{r}) = E_-^0(R)\ \exp\{-y^2/L^2 - z^2\sin^2\alpha/L^2\} \qquad (55)$$

where the y axis is out of the plane of the paper, and L is the width of the injected beam profile and $E_-^0(R)$ is the electric field on the beam axis. Taking t=0 to be the time at which the electron crosses the vertical plane through the beam axis we can write the gyrofrequency as

$$\Omega(t) = \Omega_0 + v_\parallel \Omega' t \qquad (56)$$

for the small time the electron is in the wave field. Equation (56) is not valid for trapped electrons turning within the beam but in this situation the heating out of resonance effect (section 3.4) dominates. The quantity Ω_0 is the gyrofrequency at t = 0 and is given by

$$\Omega_0(v) = \frac{eB(\chi)}{m}\left\{1 - \frac{v^2}{2c^2}\right\} \qquad (57)$$

where χ is the poloidal angle at t = 0, m is the electron rest mass and we have included relativistic effects to first order in v^2/c^2.

The inhomogeneous toroidal field and the rotational transform combine to produce the parallel gyrofrequency gradient, Ω', which is given by

$$\Omega' = \frac{\partial\Omega}{\partial z} = \frac{\Omega_0(\chi)\rho\sin\chi}{qR^2(1+\varepsilon\cos\chi)} \qquad (58)$$

where ρ is the radius of the flux surface and q is the safety factor. In obtaining eq(58) we have taken the magnetic field of the tokamak to be of the form $B(\chi) = B_a\ (1 + \varepsilon\cos\chi)^{-1}$ where $B_a = B\ (\chi = \pi/2)$. Using eq (56) the phase integral in eq (53) becomes

$$\int_{-\infty}^{t} \Omega dt' = \phi + \Omega_0 t + \tfrac{1}{2} v_{\parallel} \Omega' t^2 \qquad (59)$$

where $\phi = \int_{-\infty}^{0} \Omega dt$. Equation (54) for $[(\Delta v_{\perp})^2]$ then becomes

$$[(\Delta v_{\perp})^2] = \frac{1}{8} \left(\frac{e}{m} \frac{1}{(\ell-1)!}\right)^2 \left(\frac{k_{\perp} v_{\perp}}{2\Omega_0}\right)^{2(\ell-1)} |E_{-}^{0}|^2 e^{-2y^2/L^2} |I|^2 \qquad (60)$$

where we have taken $v_{\perp}$ to be constant during the beam transit time. The integral I is given by

$$I = \int_{-\infty}^{\infty} \exp\left\{\frac{-\beta^2 z^2}{L^2} + i(k_{\parallel} z - \omega t + \ell\Omega_0 t + \tfrac{1}{2} \ell v_{\parallel} \Omega' t^2)\right\} dt \qquad (61)$$

where $\beta = \sin\alpha$. The integration variable is now changed from t to z as follows. First we note that

$$v_{\parallel} = \sigma v \left\{1 - \frac{v_{\perp 0}^2 B(\chi)}{v^2 B(0)}\right\}^{\frac{1}{2}} \text{ and } \frac{d\chi}{dt} = \frac{v_{\parallel}}{qR} \qquad (62)$$

so that

$$\frac{dv_{\parallel}}{dt} = -\frac{v_{\perp 0}^2 \varepsilon (1+\varepsilon)\sin\chi}{2qR(1+\varepsilon\cos\chi)^2} \qquad (63)$$

where $\varepsilon = \rho/R$. Integrating eq(63) twice we obtain

$$z(t) = v_{\parallel} t - \frac{v_{\perp 0}^2 \varepsilon (1+\varepsilon)\sin\chi}{4qR(1+\varepsilon\cos\chi)^2} t^2 \qquad (64)$$

which, along with eq(58), gives

$$t = \frac{z}{v_{\parallel}} + \frac{v_{\perp 0}^2 (1+\varepsilon)}{4(1+\varepsilon\cos\chi)} \frac{\Omega'}{\Omega_0} \frac{z^2}{v_{\parallel}^3} \qquad (65)$$

provided $|v_{\parallel}|$ is sufficiently large to make the second term a correction term. Electrons with small $|v_{\parallel}|$ are dealt with in section 3.4. Hence to first order in Ω', I becomes

$$I = \int_{-\infty}^{\infty} v_{\parallel}^{-1} \exp\left\{\frac{-\beta^2 z^2}{L^2} - i\left(\frac{\omega - \ell\Omega_0}{v_{\parallel}} - k_{\parallel}\right)z + i\frac{\ell\Omega_T'}{2v_{\parallel}} z^2\right\} dz \qquad (66)$$

where
$$\Omega_T' = \Omega'\left\{1 - \frac{(\omega - \ell\Omega_0)(1+\varepsilon)v_{\perp 0}^2}{2\ell\Omega_0 (1+\varepsilon\cos\chi)v_{\parallel}^2}\right\} \qquad (67)$$

This integral may be evaluated analytically with the result[30]

$$|I| = \frac{\pi^{\frac{1}{2}}}{|v_{\parallel}| W^{\frac{1}{2}}} \exp\left\{-\frac{\beta^2}{4L^2W^2}\left(\frac{\omega - \ell\Omega_0}{v_{\parallel}} - k_{\parallel}\right)^2\right\} \qquad (68)$$

in which $W^2 = \beta^4/L^4 + (\ell\Omega_T'/2v_{\parallel})^2$. Thus the width of the resonance is determined by the beam width L and the variation of both the gyrofrequency and the parallel velocity during the electron's transit of the beam. Combining eqs (68) and (66) gives the value of $[(\Delta v_{\perp})^2]$ for a single pass through the RF at essentially a constant value of the poloidal angle χ, at which the particle orbit intersects the vertical plane through the beam axis.

On successive passes, each passing particle on a flux surface with irrational rotational transform will intersect this plane at different values of χ and will eventually map out the whole flux surface recording all values between $-\pi$ and π; the possibility of generating localised hot helical bands on rational q surfaces, as discussed by Dendy[31], is not treated in this paper. Similarly, trapped electrons will intersect the plane at values of χ between $-\chi_t$ and χ_t provided the 'banana' orbit drifts significantly in the toroidal direction. Thus we need to average $[(\Delta v_{\perp})^2]$ over the flux surface and the correct way to do this is to average over the canonical angle Φ as described in section 3.1. This leads to the following expression for D_0,

$$D_0 = \langle[(\Delta v_{\perp})^2]\rangle/2\tau$$

$$= \frac{1}{16\tau}\left(\frac{e}{m(\ell-1)!}\right)^2 \oint \left(\frac{k_{\perp} v_{\perp}}{2\Omega_0}\right)^{2(\ell-1)} |E_-^0|^2 e^{-2y^2/L^2} |I|^2 \frac{d\chi}{v_{\parallel}} \Big/ \left(\oint \frac{d\chi}{v_{\parallel}}\right) \qquad (69)$$

where τ is the average time between successive passes through the RF.

For the passing particles τ is obtained by noting that the poloidal component of velocity is $v_{\parallel}\rho(qR)^{-1}$ and so the time to complete a poloidal circuit is $Rq\int_{-\pi}^{\pi} v_{\parallel}^{-1} d\chi$. In this time the electron makes q passes on average through the microwave beam so that

$$\tau = R\int_{-\pi}^{\pi} \frac{d\chi}{v_\parallel} \tag{70}$$

In the case of the trapped electrons the time between transits of the RF in a given direction is the bounce time

$$\tau_b = 2qR\int_{-\chi_t}^{\chi_t} \frac{d\chi}{v_\parallel} \tag{71}$$

so long as the position of the banana orbit allows only one pass per bounce. However, if the length of the banana orbit is less than the toroidal circumference, the toroidal drift of the orbit will take the orbit out of the RF for a fraction of the time. Conversely, if the orbit length is greater than the circumference the electron will pass through the RF more than once in a bounce time. On average the number of passes per bounce in a given direction is $q\chi_t/\pi$ so that the average time τ for trapped electrons is given by

$$\tau = \frac{2\pi R}{\chi_t}\int_{-\chi_t}^{\chi_t} \frac{d\chi}{v_\parallel} \tag{72}$$

Of course in using eq(72) to calculate the value of D_o for trapped electrons we must sum contributions from transits of the RF in each direction.

3.3 Bounce Average of D_o

The evaluation of the integral over χ in eq(69) proceeds by assuming that, due to the exponential, significant contributions occur only within a small range of χ which is true provided the poloidal extent of the resonance region is less than the beam width. Thus we can evaluate several factors at the appropriate value of χ and remove them from the integral. Equation (69) can then be written

$$D_o = \frac{\pi}{16\tau}\left(\frac{e}{m}\frac{1}{(\ell-1)!}\right)^2 \left\{\left|E_-^0\right|^2 \left(\frac{k_\perp v_\perp}{2\Omega_0}\right)^{2(\ell-1)} \frac{e^{-2y^2/L^2}}{Wv_\parallel^3}\right\}_{\chi_{res}} \frac{K}{\oint d\chi/v_\parallel} \tag{73}$$

where χ_{res} is the poloidal angle at which the resonance condition is satisfied

$$\{\omega - \ell\,\Omega_0 - k_\parallel v_\parallel\}_{\chi_{res}} = 0 \tag{74}$$

and K is the integral

$$K = \int \exp\{\frac{-\beta^2}{2L^2W^2}(\frac{\omega - \ell\Omega_0}{v_\parallel} - k_\parallel)^2\} d\chi \qquad (75)$$

The limits of integration are $(-\pi,\pi)$ for passing electrons and $(-\chi_t,\chi_t)$ for trapped electrons. An analytic expression for this integral is used and is evaluated at each of the points on the mesh used to solve the Fokker-Planck equation (see section 4). The χ dependence of the integrand enters mainly through $\Omega_0(\chi)$ and $\Omega'(\chi)$. We ignore the variation of $v_\parallel$ over the small range of χ for which the integrand is large. This is a reasonable approximation except when resonance takes place close to the turning point of a banana orbit, but in this situation the heating out of resonance effect dominates (see section 3.4). Taking Ω_a to be the cyclotron frequency at $\chi = \pi/2$ we have

$$\Omega_0 = \Omega_a(v)/(1+\varepsilon\cos\chi), \qquad (76)$$

and, to first order in ε

$$\Omega_T' = \frac{\Omega_a}{qR}\varepsilon\sin\chi\{1 - \frac{k_\parallel v_{\perp 0}^2}{2\ell\Omega_a v_\parallel}\} \qquad (77)$$

and

$$\frac{\omega - \ell\Omega_0}{v_\parallel} - k_\parallel = \frac{\ell\Omega_a\varepsilon}{v_\parallel}(\cos\chi - H) \qquad (78)$$

where $H = \frac{1}{\varepsilon\ell\Omega_a}(k_\parallel v_\parallel + \ell\Omega_a - \omega)$ (79)

Equation (75) now becomes

$$K = \int \exp\{\frac{-C(\cos\chi - H)^2}{A + \sin^2\chi}\} d\chi \qquad (80)$$

in which

$$A = \frac{4\beta^4 v_\parallel^2 q^2 R^2}{L^4 \ell^2 \Omega_a^2 \varepsilon^2 \delta^2} \qquad (81)$$

$$C = \frac{2\beta^2 q^2 R^2}{L^2\delta^2} \qquad (82)$$

and

$$\delta = 1 - \frac{k_\parallel v_{\perp 0}^2}{2\ell\Omega_a v_\parallel} \qquad (83)$$

First we consider the case of $|H|<1$ which corresponds to an electron satisfying the resonance condition at some point on the flux surface. We expand about $\chi = \chi_{res}$ to obtain

$$\cos\chi - H = -(\chi - \chi_{res})\sin\chi_{res} - \tfrac{1}{2}(\chi - \chi_{res})^2\cos\chi_{res} + \ldots\ldots \qquad (84)$$

Substituting into eq(80) we find

$$K \simeq \pi^{\frac{1}{2}} \left[\frac{A+\sin^2\chi_{res}}{C\sin^2\chi_{res}}\right]^{\frac{1}{2}} \qquad (85)$$

except when $\sin\chi_{res}$ is sufficiently small to make the second term in eq(84) dominant. This case corresponds to resonance close to the median plane and K is given by

$$K \simeq 1.813 \left[\frac{4A}{C}\right]^{\frac{1}{4}} \qquad (86)$$

where we have used the result

$$\int_{-\infty}^{\infty} e^{-x^4} dx \simeq 1.813 \qquad (87)$$

In the code we take the smaller of the values given by eq(85) and eq(86). The case of $|H|>1$ corresponds to electrons that do not resonate on any part of the flux surface. Electrons which come closest to resonance will do so on the median plane ($|\cos\chi|=1$) and these are treated by writing

$$(H-\cos\chi)^2 \simeq (|H|-1+\chi^2/2)^2 \qquad (88)$$

which leads to

$$K = \pi^{\frac{1}{2}} \exp\left[-\frac{C(|H|-1)^2}{A}\right]\left[\frac{A}{C(|H|-1)}\right]^{\frac{1}{2}} \qquad (89)$$

Again, for the purposes of the code, we take the smaller of the values given by eq (89) and eq (86). From comparisons with calculations in which K was evaluated numerically we find that the above analytic approximations introduce inaccuracies of only a few per cent into the values of current and power absorption predicted by the code. It can be seen from eq (73) with the above expressions for K that the diffusion coefficient D_0 diverges for low values of $v_{\parallel}$. In practice, however, our assumption that the electron speed is constant is not strictly true since the electron gains or loses energy in each pass through the RF. For low values of the parallel velocity the electron can remain in the beam long enough to be heated out of resonance due to the relativistic dependence of the electron mass on energy. This effect serves to limit D_0 to finite values at low parallel velocity and an estimate of its value is given in the next section.

3.4 Heating out of Resonance

The weakly relativistic resonance condition is given by

$$v_{\parallel} k_{\parallel} \simeq \omega - \frac{\ell eB}{m} \left(1 - \frac{v_{\parallel}^2}{2c^2} - \frac{v_{\perp}^2}{2c^2}\right) \tag{90}$$

so that the electron will be heated out of resonance if the increment $\Delta v_{\perp}$ satisfies the inequality

$$\Delta v_{\perp} > \frac{mc^2}{\ell eB} \frac{v_{\parallel}}{v_{\perp}} \Delta k_{\parallel} \tag{91}$$

The spread in $k_{\parallel}$ in our model is due to the finite beam width ($\Delta k_{\parallel} \sim 2/L$) which gives

$$(\Delta v_{\perp})^2 \simeq \left(\frac{2c^2 v_{\parallel}}{L\omega v_{\perp}}\right)^2 \tag{92}$$

and an average diffusion coefficient

$$D_H = \frac{2}{\tau}\left(\frac{c^2 v_{\parallel}}{L\omega v_{\perp}}\right)^2 \tag{93}$$

However τ is no longer given by eqs(70) and (72) since it now represents the average time between resonant interactions at χ_{res} rather than the average time between transits of the RF irrespective of poloidal angle. Consider first the passing electrons which have a toroidal circulation time given by eq(70). During each transit of the RF beam these electrons sweep out a fraction $L/(2\pi Rq)$ of the flux surface poloidal circumference. Thus the average time between transits of the beam at $\chi = \chi_{res}$ is given by

$$\tau = \frac{2\pi R^2 q}{L} \int_{-\pi}^{\pi} \frac{d\chi}{v_{\parallel}} \tag{94}$$

In the case of trapped electrons, the time between successive passes through χ_{res}, irrespective of toroidal angle, is the bounce time τ_b (eq.71). However, for each electron, only a fraction $L/(2\pi R)$ of these occur within the RF beam providing the banana orbit drifts through the beam. Thus the average time between resonant interactions is

$$\tau = \frac{2\pi R}{L}\,\tau_b \qquad (95)$$

The code uses the smaller of D_H and D_o given by eq(73) on the grounds that the value of $\Delta v_\perp$ corresponding to D_o, for $D_o > D_H$, would be more than sufficient to heat the electron out of resonance. The resulting diffusion coefficient is a complex function of the velocity space variables as shown by the velocity space contour plots of D_o in Figs. 2(a) and 2(b). In order to simplify these contour plots and clarify their interpretation we have set the factor e^{-2y^2/L^2} equal to unity. Adjacent contours represent a factor of two change in the diffusion coefficient and the contour with the largest value of the coefficient has the largest label number. Both figures refer to the perpendicular injection (ie α = 0) of 60 GHz second harmonic, X-mode electron cyclotron waves into the CLEO tokamak (major radius 90 cm, minor radius 13 cm, B_a = 10.7 kG) with the resonance on the magnetic axis. Only the positive $v_{\parallel 0}$ segment is shown since the contours are symmetric about $v_{\parallel 0}$ = 0 for perpendicular injection. The calculations compare very weak (Fig 2(a), optical depth = 0) and strong absorption (Fig 2(b), optical depth = 3) and are for a flux surface radius of 3 cm and a beam width L = 5 cm which was taken from a measured TE_{11} antenna pattern.[32] For the strong absorption case, the X-mode power profile (and hence the radial dependence of E_-^o in eq (55)) was obtained from a ray tracing code[33] which incorporates the weakly relativistic expression for the dielectric tensor given by Shkarofsky[34]. Detailed methods of calculating the dielectric tensor elements and the absorption have been given by Owen[35]. In the present calculation we used temperature and density profiles of the form $T_e(\rho) = T_e(0)\{1 - (\rho/\rho_\ell)^2\}$ and $n_e(\rho) = n_e(0)\{1 - (\rho/\rho_\ell)^2\}$ where ρ_ℓ is the limiter radius. The central values were $T_e(0)$ = 1 keV and $n_e(0) = 10^{19}m^{-3}$ which gave 95% single pass absorption. The wave power, normalised to the injected power, is shown in the inset to Fig. 2 as a function of major radius.

For perpendicular injection, electrons with a given speed all come into resonance at the same value of major radius (see eq.90). Furthermore the fastest electrons come into resonance on the inside of the flux surface. In the particular case above this corresponds to electrons with v/v_e=4.13. Note that the maximum diffusion coefficients in Figs.2(a) and 2(b) occur for this value of v/v_e and also for large values of $v_{\perp o}$, as a result of the $(k_\perp v_\perp)^2$ and $(v_\parallel)^{-3}$ factors in eq(73). The decrease of the diffusion coefficient towards the trapped/passing boundary is due to the influence of D_H as the local value of $v_\parallel$ tends to zero. In the strong absorption case (Fig.2(b)) a valley appears in the contours for $v/v_e \sim 3.5$. This corresponds to electrons in resonance at R=88cm and arises due to competition between the power profile, which tends to make D_o large at low velocities, and the $v_\perp^2$ factor in eq(73) which tends to maximise D_o at large

velocities.

4. NUMERICAL SOLUTION OF THE FOKKER-PLANCK EQUATION

Numerical solutions of the Fokker-Planck equation are obtained using implicit, centred finite differencing to discretise eq(1) on a (v,θ_o) grid.[36] The grid is uniform in both co-ordinates with up to $N_v = 300$ points in velocity and $N_\theta = 100$ points in pitch angle. The maximum value of the velocity depends on the problem being solved but is typically $v_{max}/v_e \sim 8$. The boundary conditions are as follows:

$$f(v_{max}, 0) = 0 \tag{96}$$

$$\left.\frac{\partial f}{\partial \theta_o}\right|_{v=0} = 0 \tag{97}$$

$$\left.\frac{\partial f}{\partial v}\right|_{v=0,\ \theta_o=\pi/2} = 0 \tag{98}$$

$$\left.\frac{\partial f}{\partial \theta_o}\right|_{\theta_o=0,\pi} = 0 \tag{99}$$

We also ensure that $f(v,\theta_o) = f(v,\pi-\theta_o)$ in the trapped electron region and that the particles leaving the passing region enter the trapped region (or vice versa).

The resulting equations are solved directly using a Harwell subroutine[37] which efficiently inverts sparse non-symmetric matrices by means of a Gaussian elimination method. The implicit method allows steady-state solutions to be found quickly but only coarse time steps are practical if a time dependent solution is required. In the following sections the distribution function obtained is used to calculate the current density J and the density of power absorbed from the electron cyclotron waves, P_d, by numerically evaluating the integrals

$$J = -e\int v_\parallel f\, d^3v \tag{100}$$

and

$$P_d = \tfrac{1}{2} m \int v^2 \left(\frac{\partial f}{\partial t}\right)_w d^3v \tag{101}$$

Where possible the code has been tested against known results. For example, with only ohmic heating present and no trapped electrons, we obtain conductivities within 15% of the classical Spitzer-Härm[38] values. The discrepancy arises because the collision operator is not

exactly equal to the linearisation of the full non-linear operator. In addition we find that the ratio of the conductivity with trapped electrons present to that without trapping agrees with the expression $(1 - 1.95\ \varepsilon^{\frac{1}{2}} + 0.95\ \varepsilon)$ obtained by Hazeltine et al[39] to within 10% for $\varepsilon \leq 0.1$. With ECRH in the weak RF field limit we find driven currents and absorbed power densities in agreement with perturbation theory[40,41] to better than 5% for resonant velocities greater than $3v_e$. However at low resonant velocities the code underestimates the current drive efficiencies by, typically, 25% at $v_{\parallel res} \sim 0.5\ v_e$.

5. RESULTS

In the first part of this section we present ECRH current drive efficiency calculations for the COMPASS tokamak[3]. In the second part preliminary calculations of soft X-ray energy spectra are compared with a spectrum recorded during second harmonic ECRH experiments in the CLEO tokamak.[42]

5.1 Current Drive

In Fig.3 the calculated current density, J, the absorbed power density, P_d, and the current drive efficiency, J/P_d, are shown as a function of injected power, P_{inj}, for 60 GHz, second harmonic X-mode electron cyclotron waves injected into the COMPASS tokamak. The ohmic electric field is set to zero so that the effect of the RF can be seen clearly. The values of J/P_d are normalised as in ref 41. The calculations were made for an incidence angle of 70° to the field lines, a beam width, L = 5 cm, a plasma density of 1×10^{19} m^{-3} and a temperature of 1.5 keV. For each Watt of power absorbed between adjacent flux surfaces a value $J/P_d = 1$ corresponds to a current of 0.23A flowing between these flux surfaces. The wave absorption was calculated using the ray tracing code referred to in section 3.4 and the resulting wave power along the RF beam axis is shown as a function of major radius in the inset to Fig. 3. The electron cyclotron resonance was placed at R = 52 cm so that the cut off due to the relativistic mass shift occurred at the plasma centre, R = 55 cm.

The solid curves in Fig.3 refer to a flux surface with an inverse aspect ratio ε=0.08 (ρ=4.4 cm) and the dashed curve to a flux surface with ε=0.015 (ρ=0.8 cm). The most striking feature is the increase in current drive efficiency for ε=0.08 as the input power is raised. This arises because the heated passing electrons, which tend to be detuned from resonance by the relativistic mass shift, continually return to resonance at points progressively towards the inside of the flux surface (high field side) as their energy increases. This spreading of

the resonance throughout velocity space is shown by the contour plots of D_o in Fig.4(a). Thus, as the beam power is raised, larger numbers of electrons diffuse towards higher velocities thereby reducing the collisionality of the current carriers and enhancing the efficiency. This increase in efficiency contrasts with the results of preliminary calculations[7] which did not take into account the return to resonance effect.

The saturation of J, P_d and J/P_d which begins to occur at $P_{inj} \sim 2$MW is due to the heating out of resonance effect described in section 3.4. We use the smaller of D_o (which increases with P_{inj}) and D_H (which is independent of P_{inj}) so that the influence of D_H increases as the injected power is raised. Since our calculation of D_H is only approximate we expect there to be some uncertainty in the present value of the power which produces saturation. However this appears to be in excess of the maximum power of ~ 1.8 MW into the plasma envisaged for COMPASS. Contours of the electron distribution function for P_{inj} = 1.5 MW are shown in Fig. 5 and are plotted at intervals such that a Maxwellian distribution gives equally spaced semi-circles centred at the origin. Note that near the origin the distribution is indeed Maxwellian due to the small diffusion coefficient (see Fig. 4) and the large collision frequency in this region. For velocities between $4v_e$ and $8v_e$ there is a strong distortion which gives rise to the increased efficiency at high power shown in Fig. 3. For velocities greater than $8v_e$ the distortion diminishes since such energetic electrons cannot resonate on this particular flux surface of radius ρ = 4.4 cm.

The efficiency curve for the smaller flux surface, ε=0.015, ρ=0.8cm shows much less of an increase in J/P_d at high power. In this case the perpendicular velocity, $v_{\perp o}$, required to resonate on the inside of the flux surface is generally much less than the parallel velocity, $v_{\parallel o}$, as shown by the contours of D_o in Fig.4(b). Thus the collisionality of the electrons in this case is much less affected by the high power induced diffusion than in the case of ε=0.08.

The reduced efficiency on the outer flux surface is partly due to the influence of trapping and partly due to the fact that significant numbers of low energy electrons, and even electrons with negative values of $v_{\parallel o}$, can come into resonance as ε is increased (see Fig.4(a)). These effects combined with the finite beam width restrict the current to flux surfaces of radii less than 5 cm. In fact the driven current profile is hollow in this particular example because the cut-off passes through the plasma centre. Before leaving this section we note that the power absorption profile (Fig.3) given by the ray tracing could be significantly modified by both the heating out of

resonance effect and the strong distortion of the electron distribution function at high power levels. A self-consistent treatment of the power absorption is clearly desirable but requires the calculation of the distribution function, and the associated power density P_d, on each flux surface followed by iteration to find the consistent spatial variation of the wave field $E_-(\underline{r})$. A more accurate calculation of D_H than our present estimate would also be beneficial. These problems are being investigated but are beyond the scope of the present paper.

5.2 Soft X-ray Emission

The energy spectrum, $I(h\nu)$, of soft x-rays emitted from a non-isotropic electron distribution function is given by[43]

$$I(h\nu) = \frac{2\pi\zeta}{h} \sum_i n_i Z_i^2 \int_{v_\nu}^{\infty} \int_{-1}^{1} I_x \{\frac{2}{3} + (\frac{1}{3} - \cos^2\eta) P_2(\xi)\}$$

$$+ I_y \{\frac{4}{3} - (\frac{1}{3} - \cos^2\eta) P_2(\xi)\} \, fv^3 d\xi dv \qquad (102)$$

In eq(102) $h\nu$ is the photon energy, $v_\nu = (2h\nu/m)^{1/2}$, n_i is the density of ions with atomic number Z_i, η is the angle at which the photon is emitted with respect to the magnetic field, ξ is the cosine of the electron pitch angle and ζ is the solid angle subtended by the detector. Algebraic expressions are given in ref.43 for the individual polarisation intensities I_x and I_y. The predicted X-ray spectra are obtained by numerically integrating eq (102) with the distribution function f generated by the Fokker-Planck code.

A spectrum observed at 90° to the field lines during 60 GHz, second harmonic ECRH experiments in the CLEO tokamak[42] is shown in Fig.6. The experiments were made using 140kW of ECRH power and a line average density of 6×10^{18} m^{-3}. The value $Z_{eff} = 1.6$ was estimated[44] from the measured loop voltage and current using the Spitzer-Härm[38] theory of conductivity. During the RF heating period the density profile was deduced to be of the form $n_e = n_e(0) \{1-(\rho/\rho_\ell)^2\}^{2.5}$ from a self-consistent analysis involving the measurements of loop voltage, plasma current, line average density, central electron temperature, poloidal beta and soft X-ray emission profiles[44]. A best fit to the data in Fig. 6 was obtained for a temperature of 1.1 keV for the thermal background electrons and a flux surface radius of 2 cm which is consistent with the expectation that the X-ray emission is strongly weighted towards the plasma core, and with the power deposition profile predicted by ray tracing studies. Because of the distortion of the electron distribution function this best fit temperature of 1.1 keV is slightly less than the value of 1.25 keV obtained in ref 42 by fitting

the data up to 5 keV using a Maxwellian distribution. The calculated curve normalised to the data at 1.8 keV is shown in Fig. 6 and reproduces the observed spectrum. In this experiment the criterion for quasi-linear theory to hold, eq (20), is reasonably satisfied. For example we find that $(2\Delta v_\perp v_\perp / v_e^2)^2 \sim 0.2$ for $v_\perp = v_\parallel = 2\, v_e$. This preliminary analysis will be improved presently by integrating the emission along the line of sight of the detector and by representing the experimental TE_{01} radiation pattern (a hollow cone) more accurately than the Gaussian profile used so far. The spectrum observed during the ohmic heating phase is also shown in Fig. 6. The code predicts almost no distortion from Maxwellian in this case and fits the data up to the energy of the $Ti_{k\alpha}$ line.

6 Summary

A Fokker-Planck code has been developed in order to simulate and gain understanding of high power electron cyclotron heating experiments in tokamaks. The principal new features of the code are the inclusion of electron trapping and a bounce-averaged treatment of the quasi-linear diffusion operator which incorporates many of the geometrical and physics features encountered in experiments. The code has been validated against perturbation calculations, used to investigate the efficiency of ECRH current drive for the COMPASS tokamak and appears to successfully reproduce the soft X-ray energy spectrum recorded during second harmonic ECRH experiments on the CLEO tokamak.

Acknowledgement

We would like to thank Dr J B Taylor for his help in formulating the quasi-linear diffusion operator in toroidal geometry and Mr. T Edlington for making the CLEO experimental data available to us.

REFERENCES

1. V V Alikaev et al, Proc 10th Int. Conference on Plasma Physics and Controlled Nuclear Fusion Research, London 1984, (IAEA Vienna) Vol 1, 419.

2. R Prater et al, Bulletin of the American Physical Society, 29 (1984) 1427.

3. D V Bayes et al, Proc of 13th Symposium on Fusion Technology, Varese Italy 1984, Vol II p889.

4. F Söldner et al, Proc of 12th European Conference on Controlled Fusion and Plasma Physics, Budapest 1985, Vol II p244.

5. C M Bishop and R J Hastie, Nuclear Fusion 25 (1985) 1443.

6. A C Riviere et al, Proc of 4th Int. Symposium on Heating in Toroidal Plasmas, Rome 1984, Vol II p795 and references cited therein.

7. D C Robinson et al, Proc 10th Int. Conference on Plasma Physics and Controlled Nuclear Fusion Research, London 1984, Vol I p205.

8. H Hsuan et al, Proc 4th Int. Symposium on Heating in Toroidal Plasmas, Rome 1984, Vol II 809.

9. M W Alcock et al, Proc of 10th European Conf. on Controlled Fusion and Plasma Physics, Moscow 1981, Vol 1, paper H-1.

10. D C Robinson, M W Alcock, N R Ainsworth, B Lloyd and A W Morris, Proc 3rd Int Symposium on Heating in Toroidal Plasmas, Grenoble 1982, Vol II 647.

11. R M J Sillen et al, FOM Institute voor Plasmafysica Report IR 84/025, to be published in Nuclear Fusion.

12. C F F Karney and N J Fisch, Nuclear Fusion 21 (1981) 1549.

13. I Fidone, R L Meyer and G Granata, Phys. Fluids 26 (1983) 3292.

14. V V Alikaev and V L Vdovin, Sov. J. Plasma Phys. 9 (1983) 538.

15. R L Meyer, I Fidone, G Giruzzi and G Granata, Phys. Fluids 28 (1985) 127.

16. I Fidone, G Giruzzi, G Granata, V Krivenski and R L Meyer, CEA Euratom Report EUR-CEA-FC 1237 (1984).

17. J Y Hsu, V S Chan and F W McClain, Phys. Fluids 26 (1983) 3300.

18. I B Bernstein and D C Baxter, Phys Fluids 24 (1981) 108.

19. M E Mauel, Phys Fluids 27 (1984) 2899.

20. M G McCoy, G D Kerbel and R W Harvey, Comp Phys Communications, 40 (1986) 115.

21. M N Rosenbluth, R M MacDonald and D L Judd, Phys. Rev 107 (1957) 1.

22. N J Fisch and C F F Karney, Phys Fluids 24 (1981) 27.

23. G Laval and R Pellat in Physique des Plasmas, Les Houches 1972 p219, edited by C de Witt and published by Gordon and Breach 1972.

24. P J Fielding, Culham Laboratory Report CLM-P615 (1980).

25. R A Cairns and C N Lashmore-Davies, to be published in Plasma Physics.

26. A J Lichtenberg and M A Liebermann, Regular and Stochastic Motion, Springer-Verlag, 1983, p288.

27. J B Taylor, Phys. Fluids 7 (1964) 767.

28. A N Kaufman, Phys. Fluids 15 (1972) 1063.

29. Z X Zhang, M Thumm and R Wilhelm, University of Stuttgart, Institut Für Plasmaforschung report IPF-83-5 (1983).

30. I S Gradshteyn and I M Ryzhik, Tables of Integrals, Series and Products, published by Academic Press Inc. New York (1980), p485.

31. R O Dendy, Plasma Physics and Controlled Fusion 27 (1985) 1243.

32. A N Dellis and N R Ainsworth, private communication.

33. T Edlington, J G Cordey, M R O'Brien and D F H Start, Proc. 3rd Joint Varenna-Grenoble Int. Symp on Heating in Toroidal Plasmas, Grenoble 1982 Vol III, p869.

34. I P Shkarofsky, Phys. Fluids 9 (1966) 561.

35. J A Owen, Ph.D. thesis, University of St Andrews, Fife, Scotland (1985).

36. M R O'Brien, M Cox and D F H Start, Comp. Phys. Communications 40 (1986) 123.

37. I S Duff, AERE Harwell Report R11009 (1983).

38. L Spitzer and R Härm, Phys. Rev. 89 (1953) 977.

39. R D Hazeltine, F L Hinton and M N Rosenbluth, Phys Fluids 16 (1973) 1645.

40. N J Fisch and A H Boozer, Phys. Rev. Lett. 34 (1980) 720.

41. J G Cordey, T Edlington and D F H Start, Plasma Phys. 24 (1982) 73.

42. T Edlington et al, Proc. 12th European Conf. on Controlled Fusion and Plasma Physics, Budapest 1985, Vol II p 80.

43. J E Rice, K Molvig and H I Helava, Physical Review A25 (1982) 1645.

44. T Edlington, private communication.

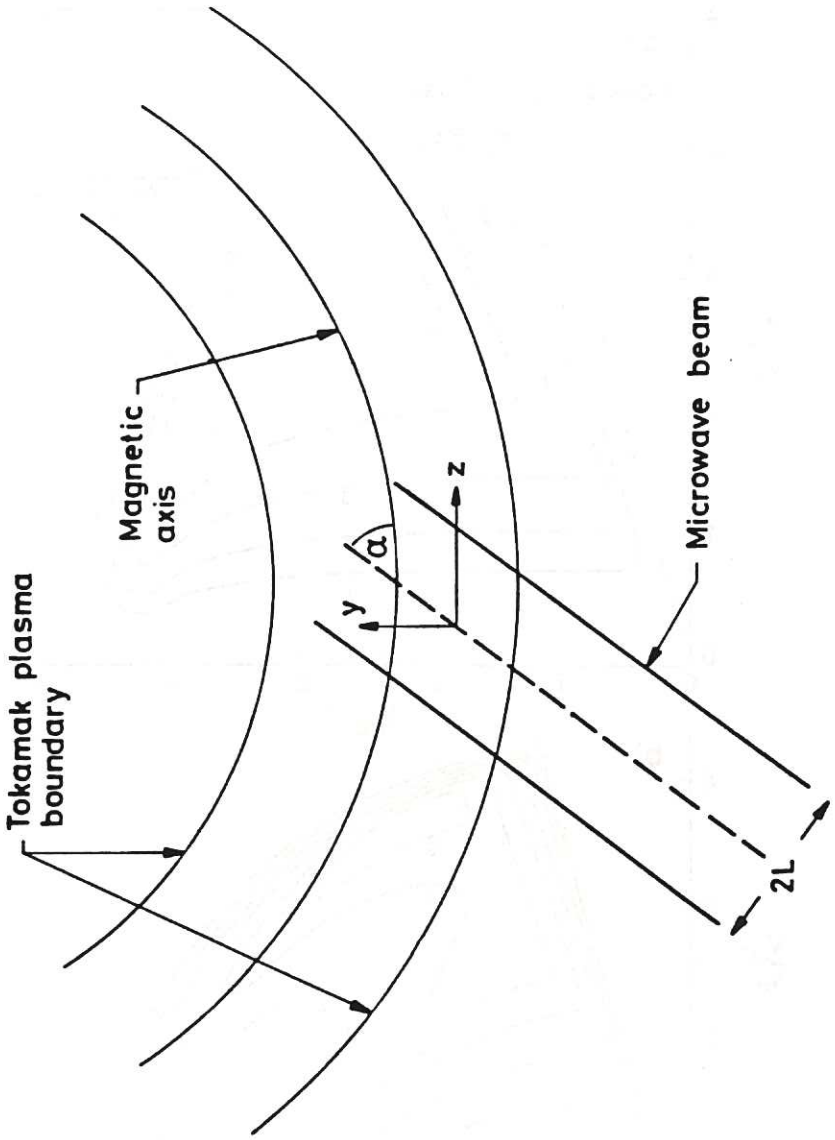

Fig. 1 Plan view of the RF injection geometry used in the present calculations. The y axis is perpendicular to the plane of the paper and the z axis lies in the median plane perpendicular to the major radius of the tokamak. The intensity of the RF beam is Gaussian in profile as given by eq. (55).

CLM-P783

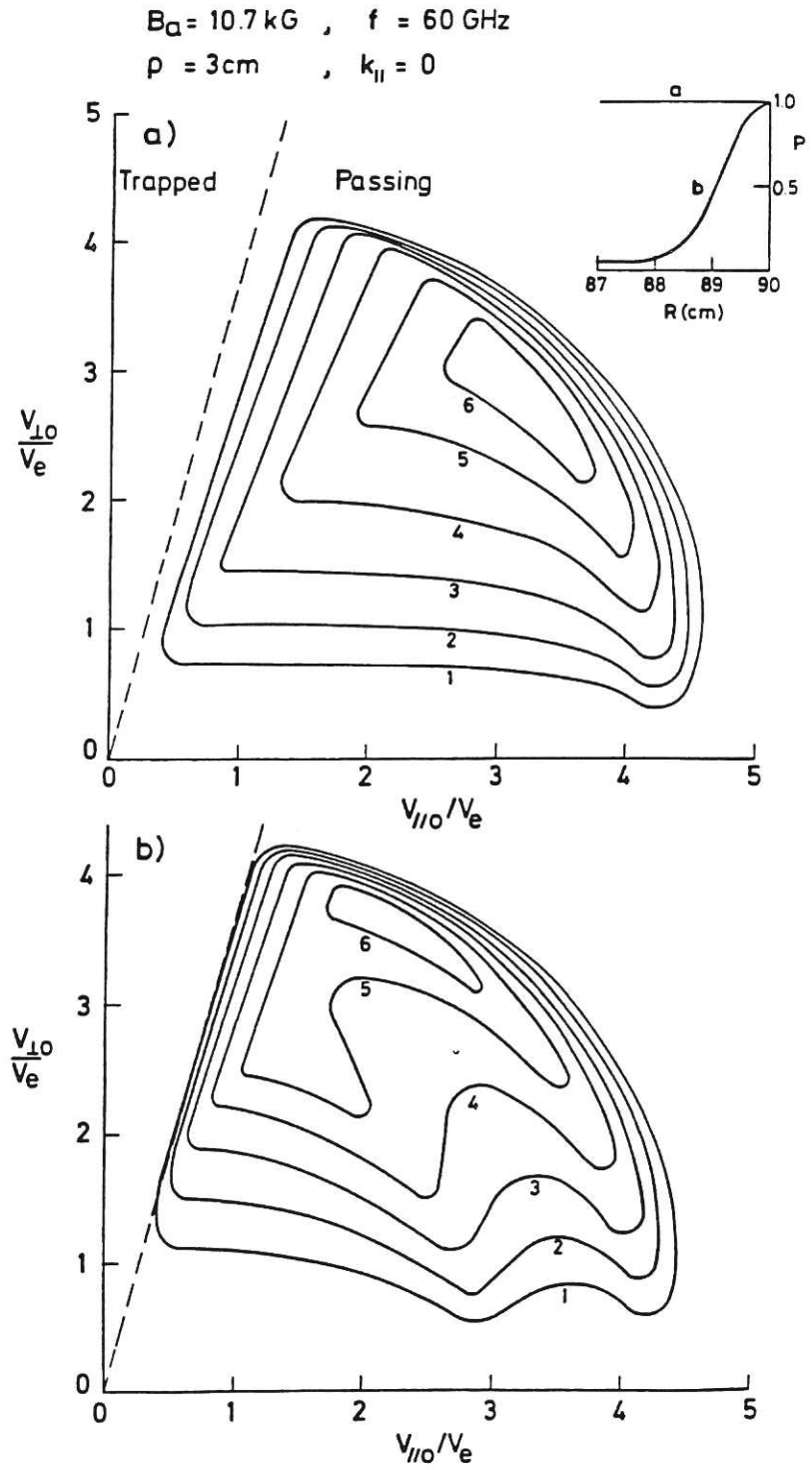

Fig. 2 Contours of the bounce averaged quasilinar diffusion coefficient D_o for weak absorption (a) and strong absorption (b) of 60 GHz, second harmonic, X-mode radiation with $k_{||}=0$ in the CLEO tokamak. The radius of the flux surface is 3 cm and the magnetic axis lies in the resonance surface (ie. $B_a=10.7$ kG). The inset shows the X-mode power in the beam as a function of major radius. For the strong absorption case (b) parabolic density and temperature profiles were used with central values $n_e(0)=10^{19}\mathrm{m}^{-3}$ and $T_e(0)=1$ keV. The contours are labelled in order of increasing values of D_o.

CLM-P783

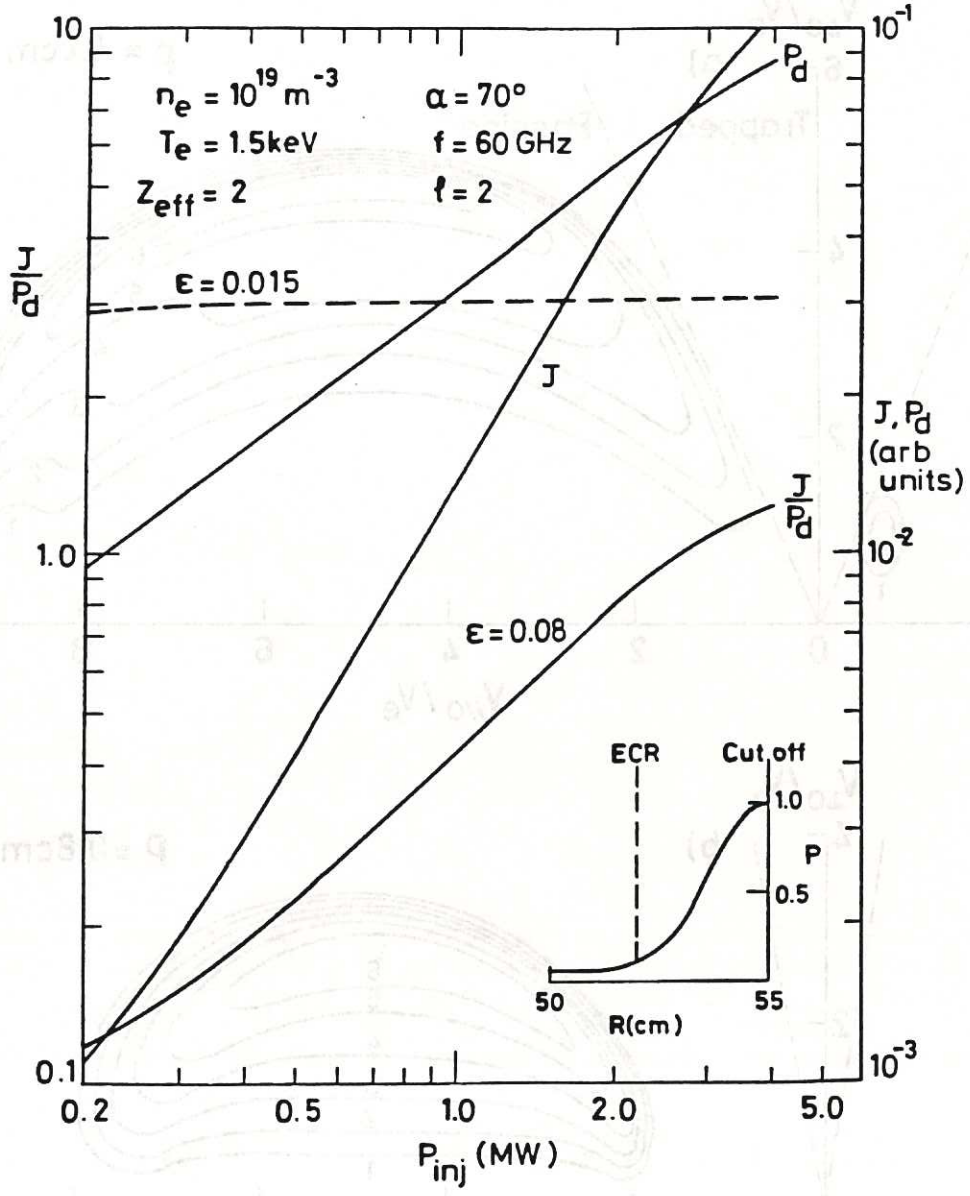

Fig. 3 Non inductive current density J, absorbed power density P_d and efficiency J/P_d plotted against injected power P_{inj} for 60GHz, second harmonic, X-mode waves injected into the COMPASS tokamak for the parameters shown in the diagram. The cyclotron resonance is placed at $R=52$cm so that the relativistic resonance cut-off occurs on the magnetic axis, R=55cm. The inset shows X-mode power as a function of major radius. The solid lines are for an inverse aspect ratio $\epsilon=0.08$. Note the increase in efficiency leading to eventual saturation as P_{inj} increases. The dashed curve shows the efficiency for $\epsilon=0.015$ for which the efficiency increase is less pronounced. The ohmic heating electric field was taken to be zero for these calculations.

CLM-P783

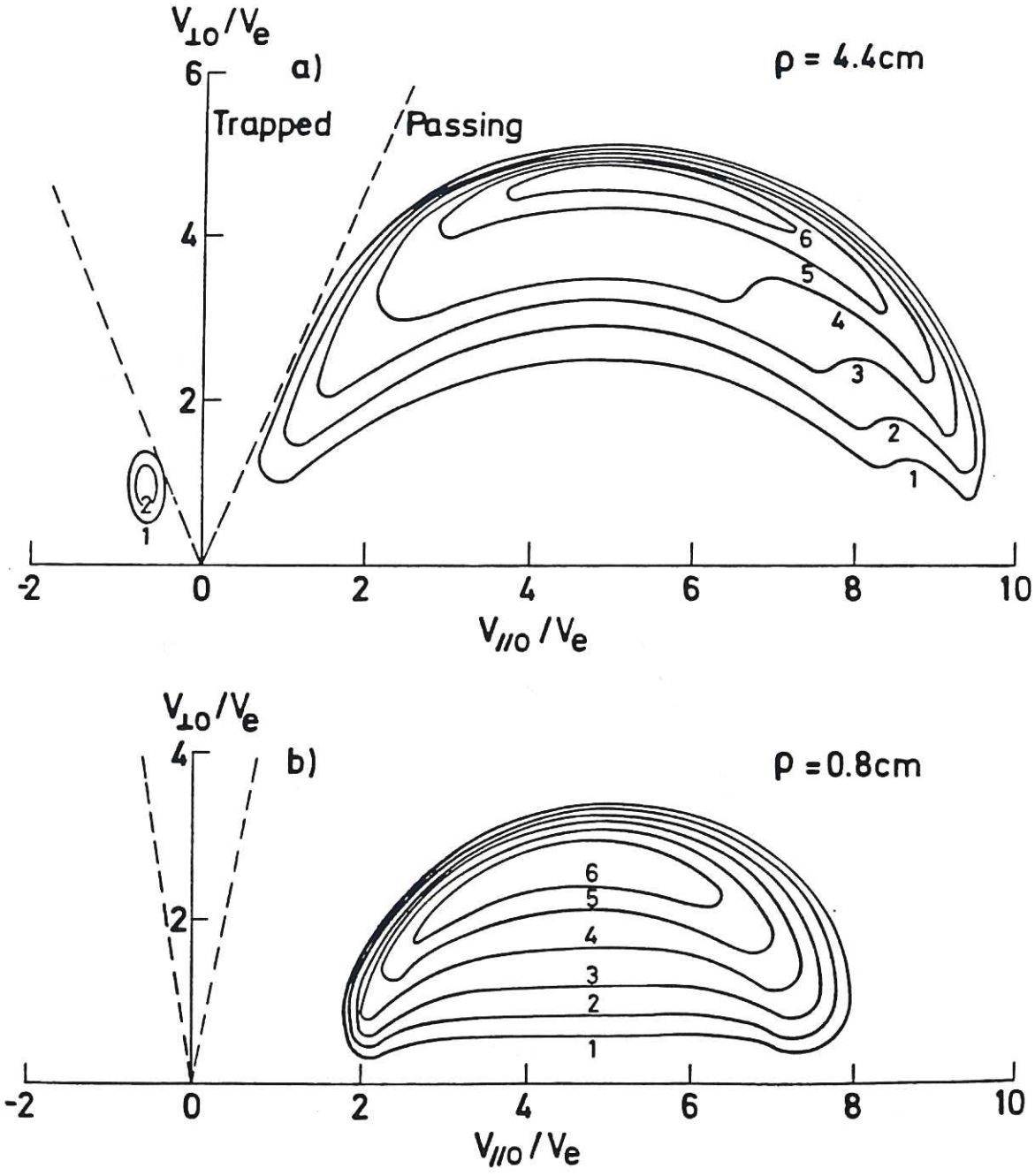

Fig. 4 Contours of D_o in velocity space corresponding to the current drive calculations shown in Fig. 3. Adjacent contours represent a factor of two change in D_o.

CLMP-783

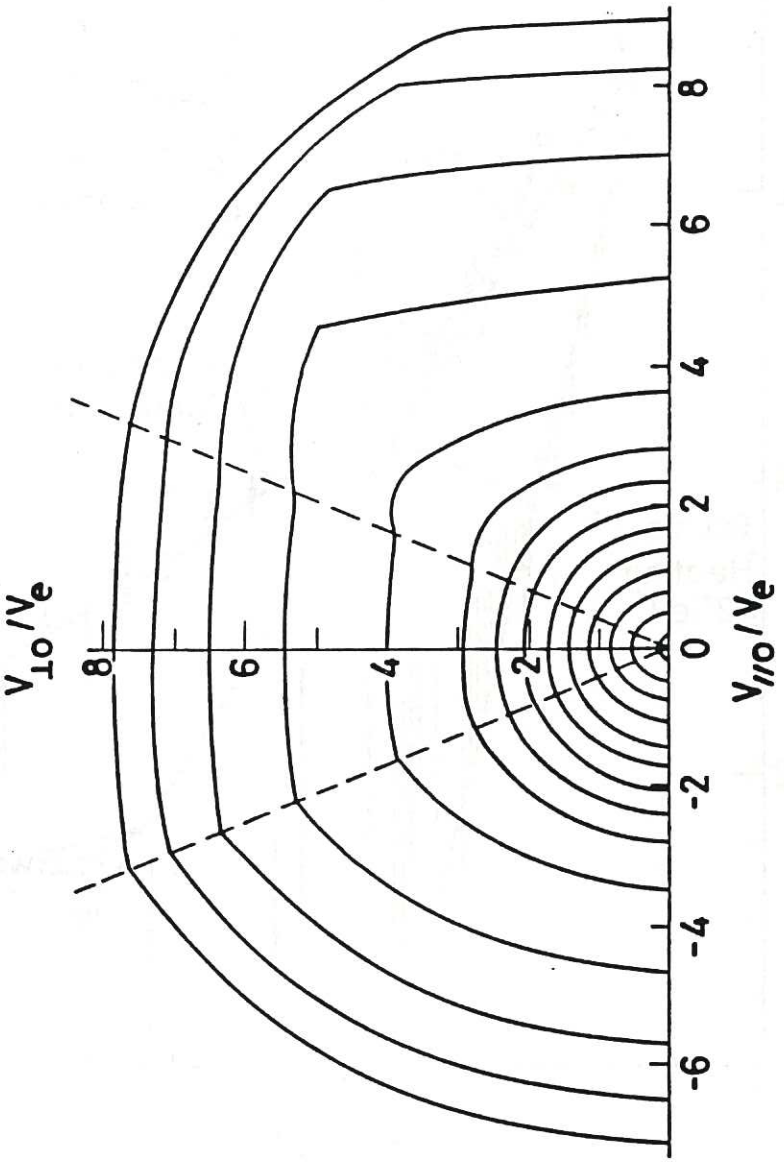

Fig. 5 Contours of the electron distribution function for the parameters pertaining to Fig. 3 and for $P_{inj}=1.5$ MW and $\epsilon=0.08$. The spacing of the contours is such that a Maxwellian gives equi-spaced semicircles centred on the origin. The dashed lines show the boundaries between trapped and passing electrons.

CLMP-783

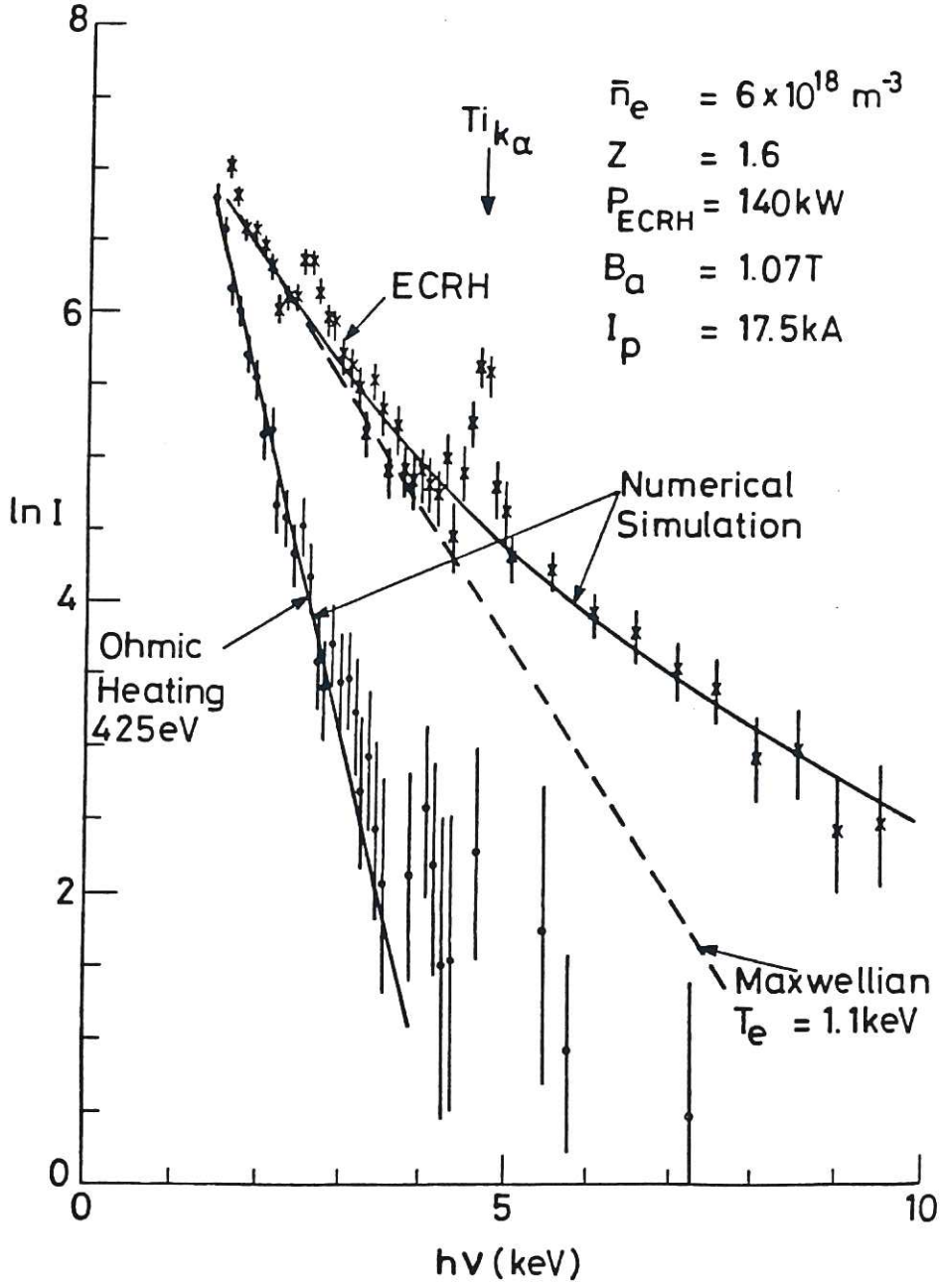

Fig. 6 Comparison of calculated and experimental soft X-ray spectra from 60GHz, second harmonic ECRH experiments on the CLEO tokamak. The calculated curve, which corresponds to a flux surface radius of 2cm, is normalised to the data at 1.8keV. The ohmic heating data taken just prior to the ECRH pulse is also shown.

CLM-P783